JCI The Journal of Clinical Investigation

Peripheral monocyte-derived cells counter amyloid plaque pathogenesis in a mouse model of Alzheimer's disease

Ping Yan, … , Jin-Moo Lee, Abhinav Diwan

J Clin Invest. 2022. https://doi.org/10.1172/JCI152565.

Research In-Press Preview **Neuroscience**

Graphical abstract

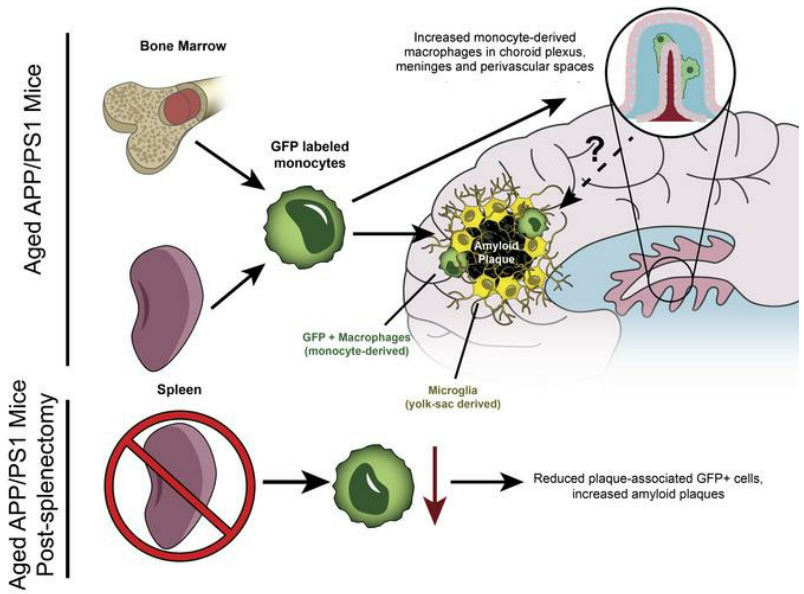

Peripheral Monocyte-derived Cells Counter Amyloid Plaque Pathogenesis in a Mouse Model of Alzheimer's Disease

Ping Yan, Ph.D. [1,2]; Ki-Wook Kim, Ph.D.[3, 4]; Qingli Xiao, Ph.D. [1,2]; Xiucui Ma, Ph.D.[5,6]; Leah Czerniewski[1,2]; Haiyan Liu, M.D.[1,2]; David R. Rawnsley, M.D., Ph.D.[5]; Yan Yan, Ph.D.[7]; Gwendalyn J. Randolph, Ph.D.[3]; Slava Epelman, MD, Ph.D.[8]*; Jin-Moo Lee, M.D., Ph.D.[1,2] *; Abhinav Diwan, M.D.[2.5,6]*

[1] Department of Neurology and [2] Hope Center for Neurological Disorders,

[3] Department of Pathology and Immunology, Washington University School of Medicine; Saint Louis, MO

[4] Department of Pharmacology and Regenerative Medicine, University of Illinois College of Medicine, Chicago, IL

[5] Department of Medicine, Washington University School of Medicine; Saint Louis, MO

[6] John Cochran VA Medical Center, St. Louis, MO;

[7] Department of Surgery, Division of Public Health Sciences, Washington University School of Medicine; Saint Louis, MO

[8] Peter Munk Cardiac Centre, University Health Network, Toronto, Ontario, Canada

* contributed equally

Address correspondence to: Abhinav Diwan, M.D., email: adiwan@wustl.edu; or, Jin-Moo Lee, M.D. Ph.D.; 660 S. Euclid Ave, CB 8111, St Louis, MO 63110, email: leejm@wustl.edu ; or Slava Epelman, M.D., Ph.D.; TMDT 3rd floor, room 903, Toronto, Ontario, Canada, M5G 1L7, email: Slava.Epelman@uhn.ca

Conflict of Interests

A.D. reports consulting for clinical trials with Clario (previously ERT/Biomedical systems) and serves on the scientific advisory board for Dewpoint Therapeutics, which are not relevant to the current study. Other authors do not have any competing interests to report.

Manuscript length (in words): 6,372

Abstract

Microglia, the parenchymal tissue macrophages in the brain, surround amyloid plaques in Alzheimer's disease (AD) but are ineffective at clearing amyloid to mitigate disease progression. Recent studies in mice indicate that microglia are exclusively derived from primitive yolk-sac hematopoiesis and self-renew without contribution from ontogenically-distinct monocytes/macrophages of definitive 'adult' hematopoietic origin. Using genetic fate-mapping to label cells of definitive hematopoietic-origin throughout the life-span, we discovered that circulating monocytes contribute 6% of plaque-associated macrophages in aged AD mice. Moreover, peripheral monocytes contributed to a higher fraction of macrophages in the choroid plexus, meninges and perivascular spaces of aged AD mice versus wild-type controls, indicating enrichment at potential sites for entry into the brain parenchyma. Splenectomy, which markedly reduced circulating Ly6C^{hi} monocytes, also reduced abundance of plaque-associated macrophages of definitive-hematopoietic origin, resulting in increased amyloid plaque load. Together, these results indicate that peripherally-derived monocytes invade the brain parenchyma, targeting amyloid plaques to reduce plaque load.

Introduction

In Alzheimer's Disease (AD), impaired clearance of Aβ peptide results in its extracellular accumulation and concentration-dependent aggregation into amyloid plaques, with neuronal toxicity (1). Microglia, the parenchymal tissue macrophages in the brain, are derived from yolk sac myeloid precursors via primitive hematopoiesis (2); and self-renew without contribution from circulating monocytes (3, 4). Microglia degrade Aβ and phagocytose amyloid material; but have been variously characterized as dysfunctional with amyloid engorgement (5), dispensable for progression of plaque pathology (6), or having a limited role in enveloping amyloid plaques to limit local Aβ diffusion and neurotoxicity with advanced AD (7, 8). Consequently, there has been tremendous interest in understanding whether ontogenically-distinct peripheral monocytes, i.e. cells derived from definitive hematopoiesis, cross the blood brain barrier to reinforce microglial function.

Early studies indicating that peripheral monocytes trafficked into the AD brain parenchyma (9, 10) were confounded by blood-brain barrier disruption induced by irradiation or chemotherapeutic regimens (9). These experimental interventions were determined to be independently sufficient to allow entry of peripheral myeloid cells into the brain (11) regardless of plaque pathology or age (9, 12). Similarly, studies implicating recruitment of peripheral monocytes based on cellular markers (13, 14) were subsequently noted to be confounded based on gene expression changes observed in these markers in disease-associated microglia in AD (15-18). Recent attempts to avoid these experimental pitfalls through a parabiosis approach did not demonstrate recruitment of peripheral monocytes; however these studies were limited to a short four-week observation window (19). Contemporary fate-mapping approaches employed tamoxifen-induced differential pulse-labeling of cells of adult hematopoietic origin (via the CCR2 promoter (20)) in the 5XFAD mouse model, characterized by rapid plaque growth (21). CCR2-promoter-driven reporter expression was observed in blood and splenic $Ly6c^{High}$ monocytes, but not in the brain parenchyma, suggesting that peripheral monocytes did not contribute to brain microglial populations in this model. However, given the short half-life of circulating monocytes (24-48 hours) (22, 23), this intermittent pulse-labeling strategy is expected to be transient, with rapid disappearance of

labeled circulating monocytes upon cessation of tamoxifen treatment, resulting in reduced sensitivity for detecting gradual monocyte invasion of the brain compared to a continuous labeling strategy. Alternate approaches to address recruitment of peripheral monocyte-derived cells such as CXCR4erT2Cre-based fate-mapping strategy in the setting of stroke (24) are not suitable due to expression of CXCR4 in microglia with amyloid pathogenesis (15, 16, 25). Towards this end, we utilized a fate-mapping approach that constitutively labels monocytes via the *Flt3* promoter (26), throughout the lifespan of the animal. We chose the APP/PS1 mouse model of AD due to clinical characteristics of slow plaque development (27), which is more reflective of human AD pathogenesis, and may provide a broader time window to allow monocyte entry.

Results

We generated male APP/PS1$^{mTmG;Flt3\text{-}Cre}$ and littermate WT$^{mTmG;Flt3\text{-}Cre}$ mice with Flt3-Cre-driven expression of dual-fluorescent mTmG reporter. *Flt3* is solely expressed in all cells of definitive hematopoietic lineage (in fetal liver, adult bone marrow and spleen) and not in yolk sac-derived microglia (3). Circulating monocytes (Ly6G^{low}CD11b+CD115+) demonstrated robust Cre-mediated GFP labeling (Fig. S1A, B), as predicted by expression of Cre via the *Flt3* promoter. Flow-cytometric immuno-phenotyping of cell-surface markers in brain macrophage isolates from mice ≥10 months of age revealed GFP expression in CD45^{high}CD11b+ cells (Fig. S2A, C), that likely include perivascular (pv), meningeal (m) and choroid plexus (cp) macrophages (MΦ); all of which are known to be maintained, in part, from contributions from adult definitive hematopoiesis-derived cells (4). GFP expression was also noted in a small fraction of CD45^{int}CD11b+ cells (Fig. S2A, D). Importantly, while we did not detect an increase in GFP+ cells among all CD45+ cellular population (Fig. S2A, B), there was a trend towards increased GFP expression in this CD45^{int}CD11b+ population (Fig. S2A, D) in APP/PS1 mice versus controls. To ascertain the location and characteristics of GFP+ cells, we employed immunohistochemistry, a gold-standard technique for examining the regional distribution of macrophage and microglia populations (4).

Histologic examination of brains from aged APP/PS1$^{mTmG;Flt3\text{-}Cre}$ and WT$^{mTmG;Flt3\text{-}Cre}$ mice (≥ 10 months of age) revealed GFP-labeled CD45+ hematopoietic cells in the choroid plexus, perivascular spaces and meninges in wild type mice (Fig. S3A, B, S4A-F). We found a significant increase in GFP-labeled CD45+ (S4A-F) and GFP-labeled CD68+ cells (Fig. 1A-F) in the choroid plexus (cpMΦ) and perivascular spaces (pvMΦ) in APP/PS1 mice as compared with wild-type controls. Notably, GFP+ cells expressing CCR2 were significantly increased in APP/PS1 mice in the choroid plexus, perivascular spaces and meninges (mMΦ; Fig. 2A-F), as compared with wild-type controls, indicating their peripheral monocyte-origin. These data point to an increased appearance of adult hematopoiesis derived monocytes/macrophages at these known transit points that permit cellular trafficking into the brain parenchyma (28).

GFP-expressing cells were observed adjacent to amyloid plaques (stained with X-34) in all aged APP/PS1 mice (>10 months of age; Fig. 3B, Table S1), but were not detected in wild-type brain parenchyma (Fig. 3A) or in 6-month old APP/PS1 mice (Table S1) at a stage prior to development of significant plaque pathology (27). Importantly, GFP-expressing cells were not observed elsewhere in the brain parenchyma of APP/PS1 mice, indicating that these cells home-in to the amyloid plaques. GFP+ cells expressed Iba1 (Fig. 3C-F), CD11b (Fig. 3G-J) and CD68 (Fig. 3K-N) and demonstrated the lack of expression of astrocyte (GFAP) and neuronal (NeuN) markers (Fig. S5). These findings indicate that the plaque-associated peripherally-derived GFP+ monocyte-derived cells had acquired characteristics of macrophages. Since *Flt3*-mediated Cre expression also labels T and B lymphocytes, neutrophils and natural killer (NK) cells (29); we examined for presence of these markers in GFP expressing cells (Fig. S6-S9). While, we detected a few GFP+ B and T cells in the choroid plexus in both genotypes, consistent with the presence of these cells in normal physiology (18) and presence of neutrophils and NK cells in the choroid plexus of APP/PS1 mice; plaque-associated GFP+ cells did not bear markers for any of these cell types.

We observed that amyloid material co-localized with plaque-associated GFP+ cells (Fig. 2O) suggesting that monocyte-derived macrophages were intimately interacting with the amyloid plaque. Quantitative examination of APP/PS1 brains revealed that the plaque-associated GFP expressing cells constitute 5.9% of all CD11b+ cells, 4.8% of CD68+ cells and 2.2% of all Iba-1 expressing cells (Tables 1, S1). There was a strong correlation between plaque load and presence of GFP+ peri-plaque cells (Fig. 3P-R), indicating that the extent of plaque pathology may influence the homing signal for these recruited cells. To rule out the possibility that the plaque-associated GFP+ peripheral monocytes are observed in APP/PS1 brains due to previously uncharacterized expression of *Flt3* in this milieu, we examined expression of FLT3 protein. We did not find any evidence to support FLT3 expression in wild type cortex or its activation in aging mice (Fig. S10).

Further characterization of plaque-associated GFP+ cells demonstrated these cells co-expressed macrophage and microglial markers such as CD45 and TREM2, a microglial protein implicated in AD pathogenesis (Fig. S11) (19). These cells were distinct from the non-plaque associated GFP+

macrophages as they lacked expression of CD206 (Fig. S11), a recently described marker enriched in non-parenchymal macrophages in the mouse brain (4). Indeed, we confirmed GFP expression in CD206+ cpMΦ and pvMΦ from both genotypes (Fig. S12), indicating adult (definitive) hematopoietic contribution to this population (4). Interestingly, GFP+ plaque-associated cells lose expression of *Ccr2* (which is observed in GFP+ cells in the perivascular spaces, meninges and choroid plexus, Fig. S13), and express *Hexb* (Fig. S14), a microglia-enriched transcript (30), which is also observed to be expressed in engrafted monocyte-derived macrophages in the brain parenchyma in the setting of experimental microglial ablation (31). Moreover, GFP+ cells in the brain parenchyma do not express *Tmem119* (Fig. S15), a microglia-enriched transcript that is detectable in APP/PS1 brains (Fig. S15) but downregulated in the 5XFAD model of accelerated amyloid pathogenesis (30). Taken together, these data suggest that peripheral monocyte derived amyloid plaque-associated cells are a unique cellular population.

Prior studies have demonstrated that the spleen contributes to definitive hematopoiesis in mice (32) and acts as a reservoir of monocytes for sustained release into the circulation with ongoing inflammatory stimuli (33). Indeed, splenic hypertrophy was observed in a triple transgenic AD model (34). Furthermore, in the post-myocardial infarction milieu, the spleen was demonstrated to a major source of circulating Ly6c^{high} monocytes (35, 36), a monocyte subset with high migratory potential into tissues (37). Indeed, splenectomy in the face of chronic stress attenuates inflammatory cell infiltration in the failing heart (38), in dystrophic muscle (39), post-stroke (40), and in abdominal aortic aneurysms (41). To determine the functional contribution of circulating monocytes to amyloid plaque pathogenesis, we performed splenectomy on male APP/PS1$^{mTmG;Flt3\text{-}Cre}$ mice. Four months after splenectomy, we observed a ~50% reduction in GFP+ cells adjacent to the amyloid plaques (Figure 4A-C), suggesting that elimination of the splenic reservoir reduced the abundance of plaque-associated macrophages of definitive hematopoiesis-origin. This result also suggests that the GFP+ macrophages in the brain parenchyma of APP/PS1 mice were peripherally-derived rather than locally proliferating GFP+ macrophages. Notably,

splenectomy did not alter the total population of peri-plaque CD11b+ cells, irrespective of the plaque size (Fig. 4D).

Given that Flt3-Cre is expressed via the Y-chromosome (29) which precludes direct examination of fate-mapping reporter system in females, we focused our analyses to evaluation of effects of splenectomy on amyloid pathogenesis in female mice. Splenectomy resulted in a significant reduction in circulating Ly6c^{High} monocytes (see Fig. 5A, B); along with neutrophils (Mean±SEM in cells/ml: 2,79,501±21,119 after splenectomy vs. 23,71,722±5,40,631 in sham; N=9-12; P=0.0002 by t-test) which are not recruited into the AD brain parenchyma (as seen in Fig. S8). Notably, splenectomy led to a modest but significant increase in HJ3.4 labeled amyloid plaque as well as in X-34-stained compact plaque in the hippocampus (Fig. 5C, D), as compared with sham controls. Splenectomy also resulted in significant increases in soluble and guanidine-extractable Aβ42 in the cortex and guanidine-extractable Aβ40 and Aβ42 in the hippocampus (Fig. 5E-H). Taken together, these data point to a functional role for circulating monocyte-derived macrophages in limiting amyloid plaque pathogenesis.

Discussion

Our data provide strong evidence that peripheral monocytes enter the AD brain and specifically home-in to amyloid plaques. The Flt3-based fate-mapping strategy overcomes the limitations of prior approaches by continuously renewed expression of the reporter in circulating monocytes in a mouse model with slower plaque growth that mimics the clinical evolution of pathology in AD. This may explain why these cells were missed in recently reported fate mapping studies that selectively labeled cells with limited life-spans (21). While the contribution of peripheral monocyte-derived macrophages to the total activated microglial/macrophage population may appear small (Table 1), it is likely that recruitment is a dynamic and ongoing process, evidenced by the increased appearance of peripheral cells at entry points to the brain (Figures 1, 2 and S4). Moreover, unlike dysfunctional microglia in aged APP/PS1 mice, which can only renew through in situ proliferation, peripherally-derived macrophages have a theoretical advantage of taking up amyloid plaque; and if toxicity occurs, to be replaced by newly formed, and fully functional macrophages.

Importantly, these peripheral monocytes migrate selectively to amyloid plaques and take on microglial markers, suggesting recruitment of newly derived macrophages (31) to reinforce microglial phagocytosis of amyloid material by virtue of being naïve to prior amyloid exposure. Indeed, our observations indicate that while splenectomy does not eliminate the circulating monocytes (with a ~53% reduction in circulating Ly6C^{High} monocytes (Fig. 5A, B)), it induces a significant reduction of ~50% in plaque-associated monocyte-derived macrophages with increased amyloid plaque pathogenesis over a period of 4 months (Fig. 5C-H). Given that splenectomy does not alter the total number of activated (CD11b+) macrophages associated with amyloid plaques (Fig. 4D), these effects of splenectomy are likely transduced by reduced monocyte recruitment into the brain parenchyma and are consistent with enhanced ability of newly recruited monocytes to degrade amyloid material as compared with the resident microglia exposed to progressive amyloid pathology.

While our data do not address the potential for pleiotropic mechanisms whereby splenectomy affects AD pathogenesis (42), these observations point to the spleen as a potential reservoir for sustained

194 recruitment of these cells to the amyloid plaques, akin to its role in other pathologic states (33, 38, 39,
195 41). Given multiple lines of evidence pointing to a role of microglial dysfunction in progression of AD
196 pathogenesis, harnessing the role of peripheral monocytes in limiting amyloid plaque pathogenesis has
197 potential therapeutic implications. Future studies will be required to assess the kinetics of peripheral
198 monocyte recruitment, survival, and proliferation in the AD brain parenchyma to comprehensively assess
199 the therapeutic potential of targeting this more accessible cellular population (as compared with
200 dysfunctional microglia confined within the brain) in prevention and treatment of AD.

Methods:

Fate mapping studies: Male APP/PS1 mice (B6;C3-Tg(APPswe,PSEN1dE9)85Dbo/Mmjax(43) from Jackson Labs, MMRRC Stock No. 34928, maintained as C57BL/6 x C3H strain) carrying the mTomato-lox-STOP-GFP cassette in the *Rosa26* locus (Jackson Labs Stock No. 007676) (44) and *Flt3* promoter driven-Cre transgene (as it is expressed on the Y-chromosome (29); RosamTmG:*Flt*3-Cre; both mice on C57BL6 strain) were generated. Littermate male mice without the APP/PS1 transgene were employed as controls. Cre-mediated excision of the mTomato cassette permits expression of GFP exclusively in monocytes, and is not observed in microglia, which are derived from primitive hematopoietic precursors in the yolk sac. Mice were sacrificed beginning at 6 months of age. After thorough perfusion with PBS to remove circulating blood cells, one brain hemisphere was homogenized, mononuclear cells isolated on a percoll gradient, as previously described (45); and live cells were evaluated using flow cytometry. The other hemisphere was used for histology. All animal studies were approved by the IACUC at Washington University School of Medicine.

Studies with splenectomy: Splenectomy or sham surgery was performed in 4.5 month-old female APP/PS1 mice (sham n=22, splenectomy n=29), following previously described surgical technique (46). The animals were randomly assigned to the splenectomy procedure. Animal are anaesthetized with the induction of Isoflurane 3-4 percent, and maintain at 2 percent. A left-side dorsal incision is made lateral to the spine and the abdominal cavity was entered. The splenic blood vessels were ligated and the spleen was removed by transecting the vessels just distal to the ligature. The skin incision is closed with wound clips. Sham surgery was performed without ligating blood vessels and spleen removing. Following surgery, mice were aged to 8.5m (± 0.5m); blood was collected for flow cytometry and brains were harvested for histological analysis. Flow cytometry of peripheral blood. Mice were cheek bled via the facial vein, and red blood cells were lysed in lysis buffer (BD Phamlyse). Nucleated peripheral blood cells were then washed once in PBS and incubated with appropriate antibodies in PBS containing 0.2% BSA

on ice for 40 min and analyzed on a FACScan flow cytometer (Becton Dickinson, Mountain View, CA). Fluorescence data were analyzed by FlowJo, BD FACS Diva analysis software. The following mixture of antibodies was used for flow cytometry: FITC anti-mouse CD11b Bioscience; APC anti-mouse CD115 Bio legend; APC-cy7 anti-mouse Ly6G; PE anti-mouse CD43 Bioscience; PerCP-cy5.5 anti-mouse Ly6c Bioscience; Pacific Blue anti-mouse CD45 Bio legend. In a separate cohort, splenectomy was performed in male APP/PS1 mice carrying the mTomato-loxp-STOP-GFP cassette in the Rosa26 locus and Flt3 promoter driven-Cre transgene at ~5.5 months of age and brains harvested at 9.5 months of age to assess for presence of GFP+ cells adjacent to plaques.

Flow cytometry: Mice were cheek-bled via the facial vein in 20ul of EDTA (100mM) and red blood cells were lysed in lysis buffer (BD Pharmlyse). Nucleated peripheral blood cells were then washed once in PBS and incubated with appropriate antibodies in PBS containing 0.2% BSA on ice for 20min and cells were analyzed on a Fortessa or LSR II (Becton Dickinson, Mountain View, CA). Blood monocytes were stained by Pacific Blue anti-CD45 (30-F11, Biolegend), APCCy7anti-CD11b (M1/70, Biolegend), APC anti-CD115(AFS98, eBioscience) and PerCP anti-Ly6C (HK1.4, Biolegend). Brain parenchymal cells were stained by Pacific Blue anti-CD45, APCCy7 anti-CD11b and PECy7 anti-Ly6G (1A8, Biolegend). Flow cytometric data were analyzed by FlowJo, BD FACS Diva analysis software.

Immunohistochemistry: Brains were perfused, removed and divided into hemispheres. One hemisphere was fixed for 24 h in 4% paraformaldehyde fixative in 0.1M phosphate buffer (PB, pH7.4), then transferred to a solution containing 30% sucrose in 0.1M PB overnight. The tissue was then sectioned (30μm) and immunostained using antibodies delineated below. Brain sections were permeabilized and blocked with 0.3% Triton X-100/ 3% dry milk in 0.01 M PBS for 30 min followed by incubation with primary antibodies overnight at 4°C; and fluorescently labeled secondary antibodies at 37°C for 1 hour. Primary and secondary antibodies employed are shown in Supplementary Table S3. GFP-tagged cells in the cortex, immunostained with Iba1 or CD11b, were counted in six equal spaced sections, and expressed

as a % of the total number of Iba1 and CD11b cells per section. Slides were mounted and examined with a Nikon A1Rsi Confocal Microscope (Washington University Center for Cellular Imaging). In control sections, the primary antibody was substituted by 3% dry milk in 0.01M PBS. GFP-tagged cells in the cortex, (which are near the amyloid plaques) were immunostained with iba1, CD11b or CD68; counted in three equal spaced sections (180 μm apart), and expressed as a % of the total number of Iba1, CD11b and CD68 expressing cells per section. For analysis of GFP-tagged cells in the choroid plexus, meningeal and peri-vascular structures, GFP+ cells were expressed as a % of total CD45 or CD68 expressing cells.

Assessment of amyloid plaques: For x34 staining, brain slices were mounted on glass slides. Tissue was permeabilized with 0.25% Triton for 30 min and stained with X-34 dissolved in a solution of 40% ethanol in water, pH 10, for 20 min. Tissue was then rinsed in distilled water and mounted. For amyloid staining, sections were permeabilized with 0.3% Tween-20 in Tris-buffered saline (TBS-T20) for 10 min, and endogenous peroxidase activity was quenched by a 10-min treatment of 0.3% H2O2 solution in TBS. Tissue was washed with TBS, blocked with 3% dry milk in TBS-T20 for 1 h, and incubated with anti-Aβ antibody (HJ3.4, 1:1000) antibody overnight. A fresh solution of streptavidin and horseradish peroxidase-conjugated biotin (1:400, Vector Laboratories, Burlingame, CA, USA) was applied to tissue for 90 min, followed by 0.025% 3-3′-diaminobenzadine tetrachloride in 0.25% NiCl and 0.05% H2O2 for 10 min. The plaque load in six equal spaced sections (180 μm apart) per mouse were analyzed and expressed as % area of the cortex.

In situ hybridization by RNAscope technology: RNAscope Multiplex Fluorescent Assay was combined with immunofluorescence technique to detect transcripts for *Tmem119*; *Ccr2* and *Hexb*, in concert with imaging amyloid plaques (HJ3.4 antibody) and microglia (iba1 antibody) in the mouse brain tissue. The RNA scope Probe for *Ccr2* gene is Mus musculus chemokine (C-C motif) receptor 2 (Ccr2) mRNA, Cat# 501681, Advanced Cell Diagnostics, Inc. Newark, CA. The RNA scope Probe for *Tmem119* gene is Mus musculus transmembrane protein 119 mRNA Cat# 472901-C2, Advanced Cell Diagnostics, Inc. Newark,

CA; and the RNA scope Probe for *Hexb* gene is Mus musculus hexosaminidase B (Hexb), mRNA, Cat# 314231-C1, Advanced Cell Diagnostics, Inc. Newark, CA. For fluorescent detection of mRNA signals, the fluorophores Opal 570 1:2000 (Opal570 reagent Pack, PN FP1488001KT) and Opal 520 1:2000 (PN FP1487001KT, Akoya Biosciences Ins. Marlborough, MA) were used. Based on the manufacturer's fixed frozen tissue protocol, mouse brain cryostat sections (30-µm thickness) post-fixation, were processed for target retrieval, protease treatment, hybridization with target probes, preamplifier, amplifier, and Opal dye incubation (RNAscope Multiples Fluorescent Reagent Kitv2 Assay, ACD, CA, USA). Briefly, after fixation in 4% paraformaldehyde in 0.1M PB for 40min, brain sections were incubated in citrate buffer (10 nmol/L, pH 6) maintained at a boiling temperature (100°C to 103°C) using a hot plate for 10 minutes, rinsed in deionized water, and immediately treated with RNAscope protease III at 40°C for 30 minutes. Hybridization with probes was performed for 2hr at 40°C follow by a serial RNAscope Multiplex FFLv2 AMP steps at 40°C for 30min, 30min and 15min respectively. Opal Dye fluorophore was applied on the sections at 40°C for 30min. After RNAscope staining, the sections were processed for fluorescence immunohistochemistry staining. The RNAscope 3-plex Negative control probe and the RNAscope 3-plex positive control probe were used to assess both tissue RNA integrity, assay procedure and background signals. Microscopic Imaging Nikon A1Rsi Confocal Microscope (Nikon, Tokyo, Japan) for imaging and analysis. Analysis of GFP+CCR2+ cells in the choroid plexus, meningeal and peri-vascular structures was performed in 4 sections/mouse and reported per unit area.

Biochemical assessment of Aβ levels: To measure Aβ, dissected cortices or hippocampi were homogenized in PBS and then in 5M guanidine in TBS, pH 8.0 (to extract fibrillar and membrane bound Aβ). $A\beta_{x-40}$ and $A\beta_{x-42}$ were assessed using mouse monoclonal capture antibodies HJ2 (anti-Aβ35–40) and HJ7.4 (anti-Aβ37–42), respectively, and a biotinylated central domain antibody, HJ5.1 (anti-Aβ13–28) was used as the detecting antibody, followed by streptavidin-poly-HRP-40 (Fitzgerald Industries), as previously described (47). All ELISA assays were developed using Super Slow ELISA TMB (Sigma) and

absorbance read on a Bio-Tek Epoch plate reader at 650 nm. Standard curves were generated from synthetic human $A\beta_{1-40}$ or $A\beta_{1-42}$ peptides (American Peptide).

Statistical analysis: Results are expressed as mean ± standard error of the mean (SEM). Assumptions of normality were examined by visual display and Shapiro-Wilks test. Log transformation to natural base was applied for data that were not normally distributed. Statistical differences were assessed with the unpaired 2-tailed Student's t-test for two experimental groups (Prism, Version 5.2) for data that were normally distributed. For data that failed normality testing, Wilcoxon rank sum test was employed. For dataset with small sample size (Fig. 2D), a permutation test was used to compare the mean between 2 groups (independence_test () in R package coin) (48). A two-tailed P value of less than 0.05 was considered statistically significant.

Study Approval: All animal studies were approved by the institutional animal use and care committee (IACUC) at Washington University School of Medicine.

Author's contributions

P.Y. and K-W. K. performed experiments, acquired, analyzed and collated the data, and assisted with manuscript preparation; Q.X., X.M., D.R.R., L.C., and H.L. performed experiments, and acquired and analyzed the data; Y.Y. analyzed the data; and G.J.R., S.E., J-M.L., and A.D. designed the study and wrote the manuscript. All authors read and approved the final manuscript.

Acknowledgements:

This study was supported by grants from the NIH (R01 NS094692) to J-M. L. and A.D.; from the NIH (R21 NS082529) to J-M.L.; from the Alzheimer's Association (NIRG 12-242588) and from the NIH (R01 HL107594) to A.D.; from the NIH (R01 DK126753) to K-W.K.; and from the NIH (R37 AI049653) to G.J.R. D.R.R. was supported by a grant from the National Institutes of Health (T32 HL007081). This work was supported by the Hope Center Viral Vectors Core at Washington University School of Medicine.

391 References
392
393 1. Musiek ES, and Holtzman DM. Three dimensions of the amyloid hypothesis: time, space and
394 'wingmen'. *Nature neuroscience.* 2015;18(6):800-6.
395 2. Ginhoux F, Greter M, Leboeuf M, Nandi S, See P, Gokhan S, et al. Fate mapping analysis reveals
396 that adult microglia derive from primitive macrophages. *Science.* 2010;330(6005):841-5.
397 3. Epelman S, Lavine KJ, and Randolph GJ. Origin and functions of tissue macrophages. *Immunity.*
398 2014;41(1):21-35.
399 4. Goldmann T, Wieghofer P, Jordao MJ, Prutek F, Hagemeyer N, Frenzel K, et al. Origin, fate and
400 dynamics of macrophages at central nervous system interfaces. *Nature immunology.*
401 2016;17(7):797-805.
402 5. Lucin KM, O'Brien CE, Bieri G, Czirr E, Mosher KI, Abbey RJ, et al. Microglial beclin 1
403 regulates retromer trafficking and phagocytosis and is impaired in Alzheimer's disease. *Neuron.*
404 2013;79(5):873-86.
405 6. Aguzzi A, Barres BA, and Bennett ML. Microglia: scapegoat, saboteur, or something else?
406 *Science.* 2013;339(6116):156-61.
407 7. Condello C, Yuan P, Schain A, and Grutzendler J. Microglia constitute a barrier that prevents
408 neurotoxic protofibrillar Abeta42 hotspots around plaques. *Nat Commun.* 2015;6:6176.
409 8. Yuan P, Condello C, Keene CD, Wang Y, Bird TD, Paul SM, et al. TREM2 Haplodeficiency in
410 Mice and Humans Impairs the Microglia Barrier Function Leading to Decreased Amyloid
411 Compaction and Severe Axonal Dystrophy. *Neuron.* 2016;90(4):724-39.
412 9. Simard AR, Soulet D, Gowing G, Julien JP, and Rivest S. Bone marrow-derived microglia play a
413 critical role in restricting senile plaque formation in Alzheimer's disease. *Neuron.*
414 2006;49(4):489-502.

10. El Khoury J, Toft M, Hickman SE, Means TK, Terada K, Geula C, et al. Ccr2 deficiency impairs microglial accumulation and accelerates progression of Alzheimer-like disease. *Nature medicine.* 2007;13(4):432-8.

11. Mildner A, Schmidt H, Nitsche M, Merkler D, Hanisch UK, Mack M, et al. Microglia in the adult brain arise from Ly-6ChiCCR2+ monocytes only under defined host conditions. *Nature neuroscience.* 2007;10(12):1544-53.

12. Mildner A, Schlevogt B, Kierdorf K, Bottcher C, Erny D, Kummer MP, et al. Distinct and non-redundant roles of microglia and myeloid subsets in mouse models of Alzheimer's disease. *The Journal of neuroscience : the official journal of the Society for Neuroscience.* 2011;31(31):11159-71.

13. Jay TR, Miller CM, Cheng PJ, Graham LC, Bemiller S, Broihier ML, et al. TREM2 deficiency eliminates TREM2+ inflammatory macrophages and ameliorates pathology in Alzheimer's disease mouse models. *The Journal of experimental medicine.* 2015;212(3):287-95.

14. Korin B, Ben-Shaanan TL, Schiller M, Dubovik T, Azulay-Debby H, Boshnak NT, et al. High-dimensional, single-cell characterization of the brain's immune compartment. *Nature neuroscience.* 2017;20(9):1300-9.

15. Keren-Shaul H, Spinrad A, Weiner A, Matcovitch-Natan O, Dvir-Szternfeld R, Ulland TK, et al. A Unique Microglia Type Associated with Restricting Development of Alzheimer's Disease. *Cell.* 2017;169(7):1276-90.e17.

16. Krasemann S, Madore C, Cialic R, Baufeld C, Calcagno N, El Fatimy R, et al. The TREM2-APOE Pathway Drives the Transcriptional Phenotype of Dysfunctional Microglia in Neurodegenerative Diseases. *Immunity.* 2017;47(3):566-81.e9.

17. Lund H, Pieber M, Parsa R, Han J, Grommisch D, Ewing E, et al. Competitive repopulation of an empty microglial niche yields functionally distinct subsets of microglia-like cells. *Nat Commun.* 2018;9(1):4845.

18. Mrdjen D, Pavlovic A, Hartmann FJ, Schreiner B, Utz SG, Leung BP, et al. High-Dimensional Single-Cell Mapping of Central Nervous System Immune Cells Reveals Distinct Myeloid Subsets in Health, Aging, and Disease. *Immunity.* 2018;48(2):380-95.e6.

19. Wang Y, Ulland TK, Ulrich JD, Song W, Tzaferis JA, Hole JT, et al. TREM2-mediated early microglial response limits diffusion and toxicity of amyloid plaques. *The Journal of experimental medicine.* 2016;213(5):667-75.

20. Croxford AL, Lanzinger M, Hartmann FJ, Schreiner B, Mair F, Pelczar P, et al. The Cytokine GM-CSF Drives the Inflammatory Signature of CCR2+ Monocytes and Licenses Autoimmunity. *Immunity.* 2015;43(3):502-14.

21. Reed-Geaghan EG, Croxford AL, Becher B, and Landreth GE. Plaque-associated myeloid cells derive from resident microglia in an Alzheimer's disease model. *The Journal of experimental medicine.* 2020;217(4).

22. Yona S, Kim KW, Wolf Y, Mildner A, Varol D, Breker M, et al. Fate mapping reveals origins and dynamics of monocytes and tissue macrophages under homeostasis. *Immunity.* 2013;38(1):79-91.

23. Patel AA, Zhang Y, Fullerton JN, Boelen L, Rongvaux A, Maini AA, et al. The fate and lifespan of human monocyte subsets in steady state and systemic inflammation. *The Journal of experimental medicine.* 2017;214(7):1913-23.

24. Werner Y, Mass E, Ashok Kumar P, Ulas T, Händler K, Horne A, et al. Cxcr4 distinguishes HSC-derived monocytes from microglia and reveals monocyte immune responses to experimental stroke. *Nature neuroscience.* 2020;23(3):351-62.

25. Krauthausen M, Kummer MP, Zimmermann J, Reyes-Irisarri E, Terwel D, Bulic B, et al. CXCR3 promotes plaque formation and behavioral deficits in an Alzheimer's disease model. *The Journal of clinical investigation.* 2015;125(1):365-78.

26. Boyer SW, Schroeder AV, Smith-Berdan S, and Forsberg EC. All hematopoietic cells develop from hematopoietic stem cells through Flk2/Flt3-positive progenitor cells. *Cell Stem Cell.* 2011;9(1):64-73.

27. Yan P, Bero AW, Cirrito JR, Xiao Q, Hu X, Wang Y, et al. Characterizing the appearance and growth of amyloid plaques in APP/PS1 mice. *The Journal of neuroscience : the official journal of the Society for Neuroscience.* 2009;29(34):10706-14.

28. Ousman SS, and Kubes P. Immune surveillance in the central nervous system. *Nature neuroscience.* 2012;15(8):1096-101.

29. Boyer SW, Beaudin AE, and Forsberg EC. Mapping differentiation pathways from hematopoietic stem cells using Flk2/Flt3 lineage tracing. *Cell Cycle.* 2012;11(17):3180-8.

30. Masuda T, Amann L, Sankowski R, Staszewski O, Lenz M, P DE, et al. Novel Hexb-based tools for studying microglia in the CNS. *Nature immunology.* 2020;21(7):802-15.

31. Shemer A, Grozovski J, Tay TL, Tao J, Volaski A, Süß P, et al. Engrafted parenchymal brain macrophages differ from microglia in transcriptome, chromatin landscape and response to challenge. *Nat Commun.* 2018;9(1):5206.

32. Wolber FM, Leonard E, Michael S, Orschell-Traycoff CM, Yoder MC, and Srour EF. Roles of spleen and liver in development of the murine hematopoietic system. *Experimental hematology.* 2002;30(9):1010-9.

33. Swirski FK, Nahrendorf M, Etzrodt M, Wildgruber M, Cortez-Retamozo V, Panizzi P, et al. Identification of splenic reservoir monocytes and their deployment to inflammatory sites. *Science.* 2009;325(5940):612-6.

34. Yang SH, Kim J, Lee MJ, and Kim Y. Abnormalities of plasma cytokines and spleen in senile APP/PS1/Tau transgenic mouse model. *Sci Rep.* 2015;5:15703.

35. Sager HB, Hulsmans M, Lavine KJ, Moreira MB, Heidt T, Courties G, et al. Proliferation and Recruitment Contribute to Myocardial Macrophage Expansion in Chronic Heart Failure. *Circ Res.* 2016;119(7):853-64.

36. Emami H, Singh P, MacNabb M, Vucic E, Lavender Z, Rudd JH, et al. Splenic metabolic activity predicts risk of future cardiovascular events: demonstration of a cardiosplenic axis in humans. *JACC Cardiovasc Imaging.* 2015;8(2):121-30.

37. Geissmann F, Jung S, and Littman DR. Blood monocytes consist of two principal subsets with distinct migratory properties. *Immunity.* 2003;19(1):71-82.

38. Ismahil MA, Hamid T, Bansal SS, Patel B, Kingery JR, and Prabhu SD. Remodeling of the mononuclear phagocyte network underlies chronic inflammation and disease progression in heart failure: critical importance of the cardiosplenic axis. *Circ Res.* 2014;114(2):266-82.

39. Rizzo G, Di Maggio R, Benedetti A, Morroni J, Bouche M, and Lozanoska-Ochser B. Splenic Ly6Chi monocytes are critical players in dystrophic muscle injury and repair. *JCI Insight.* 2020;5(2).

40. Seifert HA, and Offner H. The splenic response to stroke: from rodents to stroke subjects. *Journal of neuroinflammation.* 2018;15(1):195.

41. Mellak S, Ait-Oufella H, Esposito B, Loyer X, Poirier M, Tedder TF, et al. Angiotensin II mobilizes spleen monocytes to promote the development of abdominal aortic aneurysm in Apoe-/- mice. *Arteriosclerosis, thrombosis, and vascular biology.* 2015;35(2):378-88.

42. Dantzer R. Neuroimmune Interactions: From the Brain to the Immune System and Vice Versa. *Physiological reviews.* 2018;98(1):477-504.

43. Jankowsky JL, Fadale DJ, Anderson J, Xu GM, Gonzales V, Jenkins NA, et al. Mutant presenilins specifically elevate the levels of the 42 residue beta-amyloid peptide in vivo: evidence for augmentation of a 42-specific gamma secretase. *Hum Mol Genet.* 2004;13(2):159-70.

44. Muzumdar MD, Tasic B, Miyamichi K, Li L, and Luo L. A global double-fluorescent Cre reporter mouse. *Genesis.* 2007;45(9):593-605.

45. Lee S, Xu G, Jay TR, Bhatta S, Kim KW, Jung S, et al. Opposing effects of membrane-anchored CX3CL1 on amyloid and tau pathologies via the p38 MAPK pathway. *The Journal of neuroscience : the official journal of the Society for Neuroscience.* 2014;34(37):12538-46.

46. Reeves JP, Reeves PA, and Chin LT. Survival surgery: removal of the spleen or thymus. *Current protocols in immunology.* 2001;Chapter 1:Unit 1.10.

47. Xiao Q, Yan P, Ma X, Liu H, Perez R, Zhu A, et al. Enhancing astrocytic lysosome biogenesis facilitates abeta clearance and attenuates amyloid plaque pathogenesis. *The Journal of neuroscience : the official journal of the Society for Neuroscience.* 2014;34(29):9607-20.

48. Hothorn T, Hornik K, van de Wiel MA, and Zeileis A. Implementing a Class of Permutation Tests: The coin Package. *Journal of Statistical Software.* 2008;28(8):1 - 23.

Figure 1

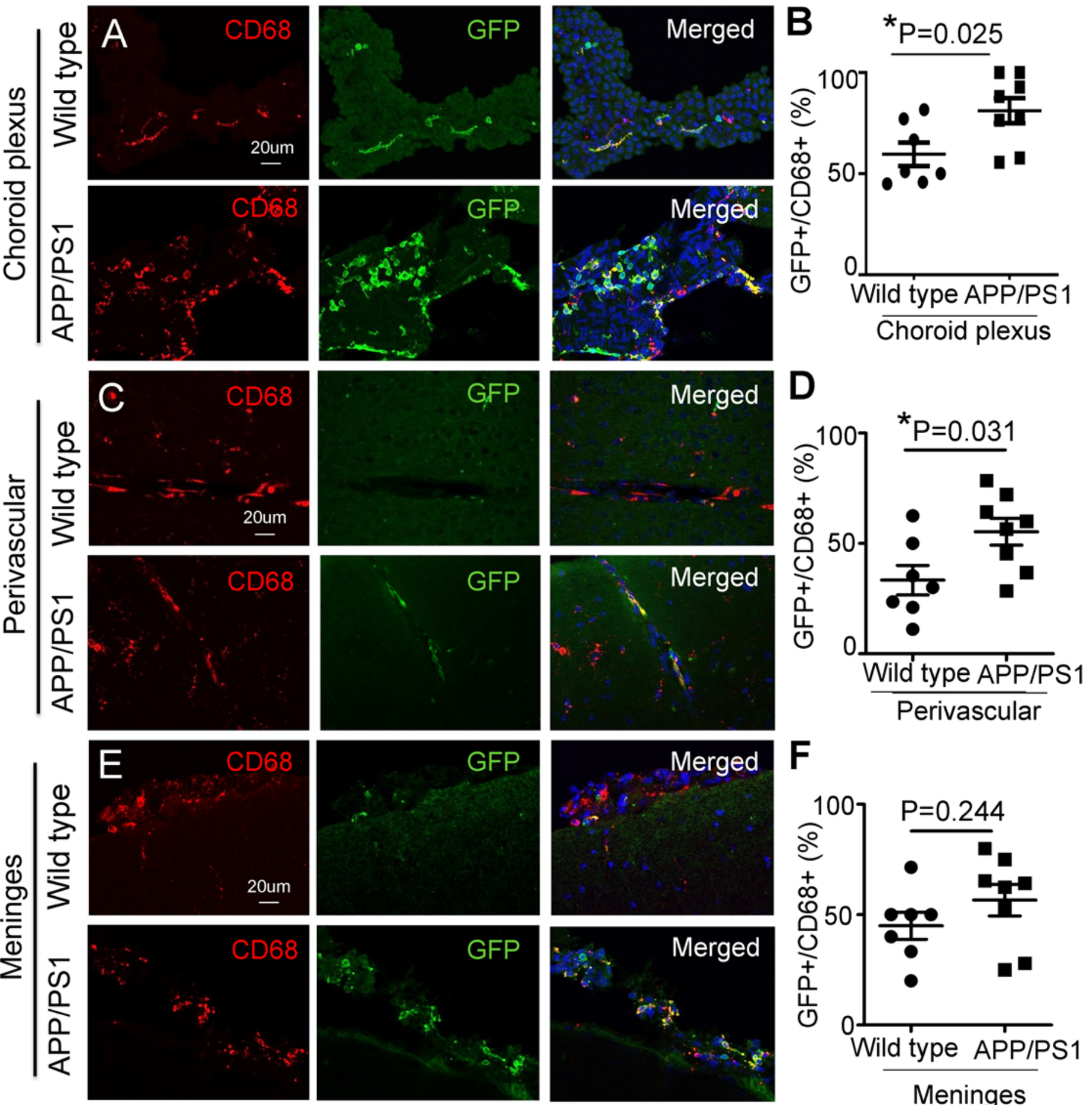
A
CD68
GFP
Merged
20um
Wild type
APP/PS1
Choroid plexus
B
*P=0.025
GFP+/CD68+ (%)
100
50
0
Wild type APP/PS1
Choroid plexus
C
CD68
GFP
Merged
20um
Wild type
APP/PS1
Perivascular
D
*P=0.031
GFP+/CD68+ (%)
100
50
0
Wild type APP/PS1
Perivascular
E
CD68
GFP
Merged
20um
Wild type
APP/PS1
Meninges
F
P=0.244
GFP+/CD68+ (%)
100
50
0
Wild type APP/PS1
Meninges

Figure 1: Fate mapping demonstrates increased contribution of adult hematopoiesis-derived cells to CD68+ macrophages in the choroid plexus and perivascular space in APP/PS1 mice. A-F. Representative images demonstrating GFP expression in CD68+ cells in WTmTmG;Flt3-Cre and APP/PS1mTmG;Flt3-Cre mice between 10-17 months of age in the choroid plexus (A), perivascular space (C) and meninges (E); with quantitation of GFP expression in this cell population in the respective populations (B, D, and F). N=7-8/group. P values are by t-test. * indicate $P<0.05$.

Figure 2

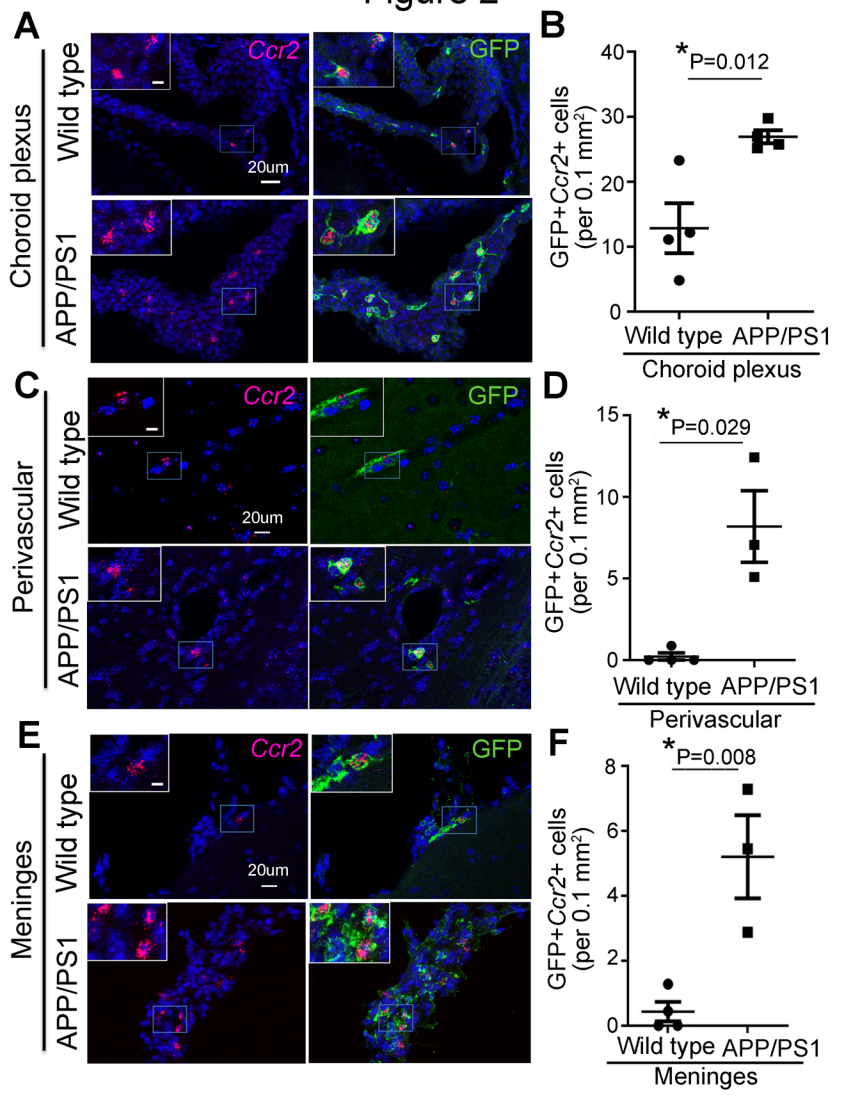
A
Choroid plexus
Wild type
APP/PS1
Ccr2
GFP
20um
B
*P=0.012
GFP+Ccr2+ cells (per 0.1 mm2)
40
30
20
10
0
Wild type
APP/PS1
Choroid plexus
C
Perivascular
Wild type
APP/PS1
Ccr2
GFP
20um
D
*P=0.029
GFP+Ccr2+ cells (per 0.1 mm2)
15
10
5
0
Wild type
APP/PS1
Perivascular
E
Meninges
Wild type
APP/PS1
Ccr2
GFP
20um
F
*P=0.008
GFP+Ccr2+ cells (per 0.1 mm2)
8
6
4
2
0
Wild type
APP/PS1
Meninges

Figure 2: Peripheral monocyte-derived cells are increased in the choroid plexus, perivascular space and meninges of APP/PS1 mice. A-F. Representative images demonstrating GFP+Ccr2+ cells in WTmTmG;Flt3-Cre and APP/PS1mTmG;Flt3-Cre mice between 10-17 months of age in the choroid plexus (A), perivascular space (C) and meninges (E); with quantitation of GFP+Ccr2+ cells in the respective locations (B, D and F). Insets in panel B are magnified images of outlined areas on the respective images. Scale bar in inset = 10μm. P values are by t-test for panels B and F, and by permutation testing for panel D (see methods). N=3-4/group.
* indicate $P<0.05$.

Figure 3

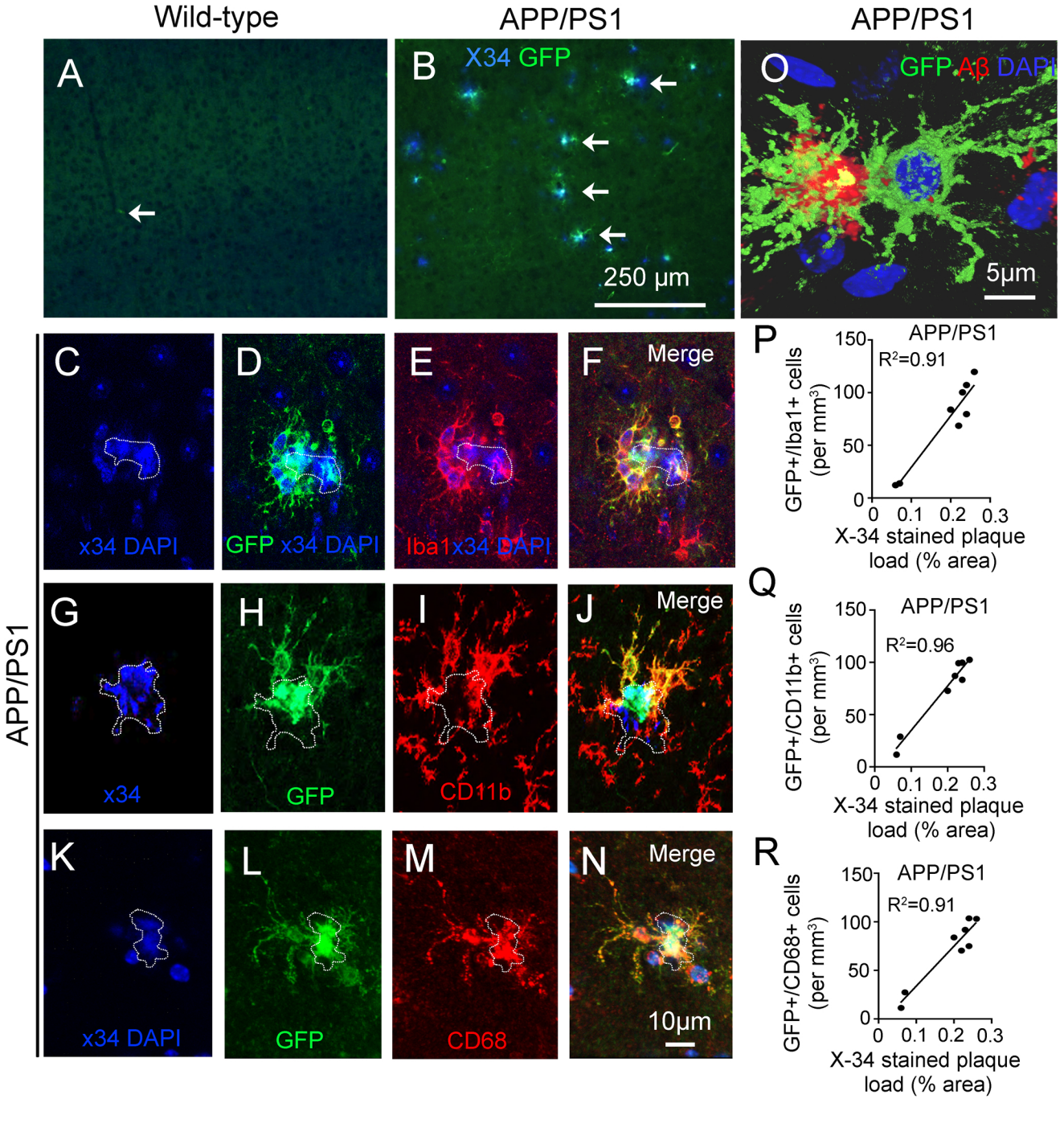
Wild-type
APP/PS1
APP/PS1
A
B
X34 GFP
250 μm
O
GFP Aβ DAPI
5μm
APP/PS1
C
x34 DAPI
D
GFP x34 DAPI
E
Iba1 x34 DAPI
F
Merge
G
x34
H
GFP
I
CD11b
J
Merge
K
x34 DAPI
L
GFP
M
CD68
N
Merge
10μm
P
APP/PS1
R²=0.91
GFP+/Iba1+ cells (per mm³)
X-34 stained plaque load (% area)
Q
APP/PS1
R²=0.96
GFP+/CD11b+ cells (per mm³)
X-34 stained plaque load (% area)
R
APP/PS1
R²=0.91
GFP+/CD68+ cells (per mm³)
X-34 stained plaque load (% area)

Figure 3: Fate mapping demonstrates peripheral monocyte-derived cells adjacent to amyloid plaques in the brain parenchyma of APP/PS1 mice. A, B. Representative cortical sections from aged WTmTmG;Flt3-Cre (n=5) and APP/PS1mTmG;Flt3-Cre mice (n=8) demonstrating that GFP+ cells are not detected in the WT brain parenchyma (A) and are seen adjacent to X-34-stained amyloid plaques in APP/PS1 mice (B). White arrows point to a GFP+ cell in the perivascular space in WTmTmG;Flt3-Cre brain in A, and to GFP+ cells adjacent to X34 labeled amyloid plaques. C-N. Representative cortical sections from aged APP/PS1mTmG;Flt3-Cre mice demonstrating X-34-stained plaque (with DAPI stained nuclei as shown, plaque is outlined) with GFP expression (D, H, L), which co-localizes with a microglial marker, Iba-1 (E, F); with CD11b, a marker for activated microglia (I, J); and with CD68, a marker for phagocytic cells also present on microglia (M, N). O. A GFP+ cell adjacent to amyloid plaque demonstrating co-localization with Aβ (red). **P-R.** Correlation between the density of GFP+ cells expressing Iba-1 (P), CD11b (Q) and CD68 (R) in the cortex and the amyloid plaque load detected by X-34 staining. Pearson's coefficient of correlation, R2 is shown with $P<0.001$.

Figure 4

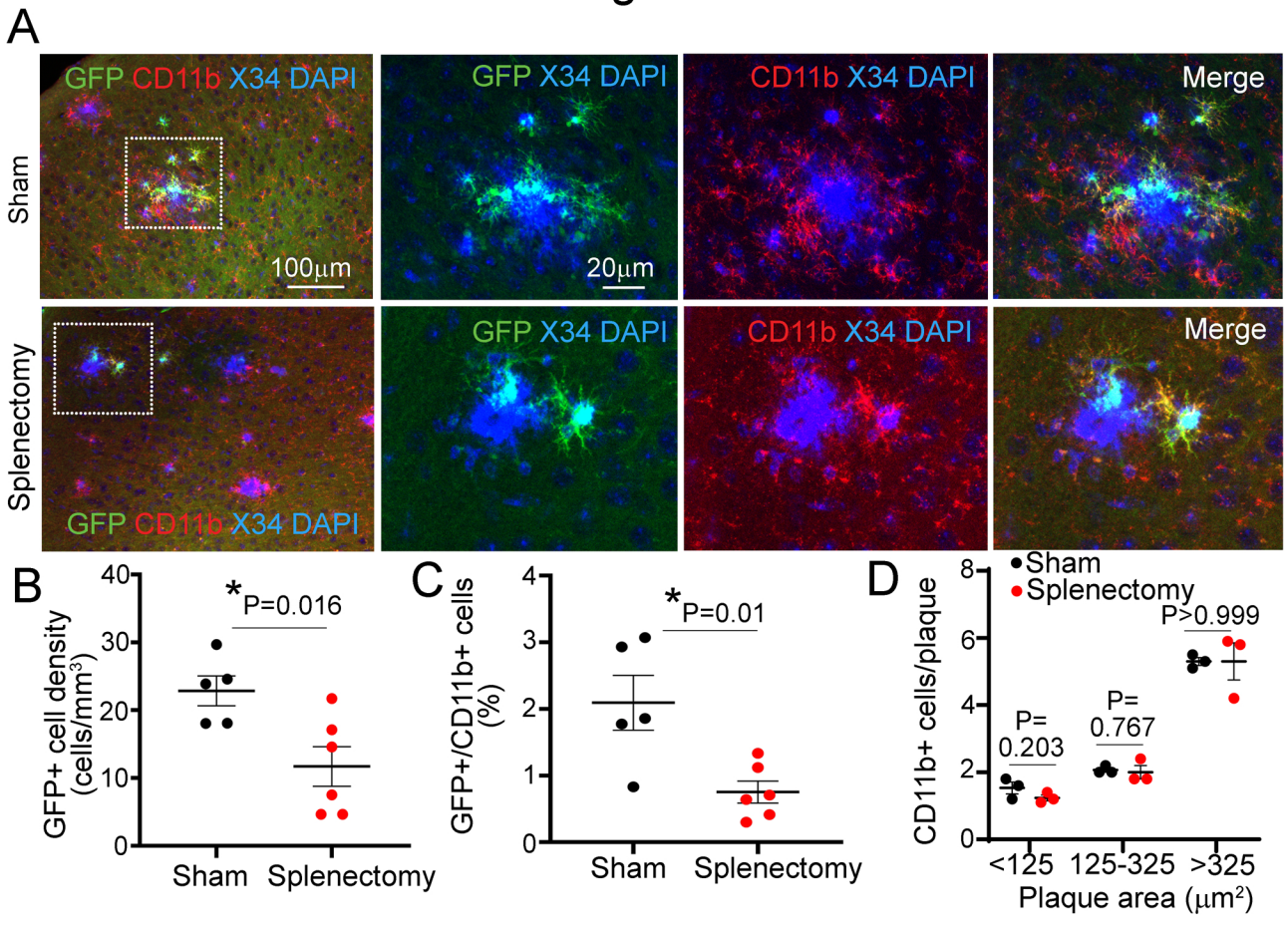

Figure 4: Splenectomy results in reduced monocyte-derived peri-plaque macrophages. Representative cortical sections from APP/PS1mTmG;Flt3-Cre mice subjected to splenectomy at 5.5 months of age and sacrificed at 9.5 months of age, demonstrating fewer GFP+ CD11b+ cells next to amyloid plaques stained with X-34. Area marked by dotted lines in left panels is magnified in the three images on the right. **B,C.** Density of GFP+ cells in the brain parenchyma cells (C) in mice from A. **D**. Abundance of CD11b+ cells adjacent to amyloid plaques stratified by size in mice from A. N=6 post-splenectomy and N=5 post-sham procedure. P values are by t-test for panels B-D. * indicate P<0.05.

Figure 5

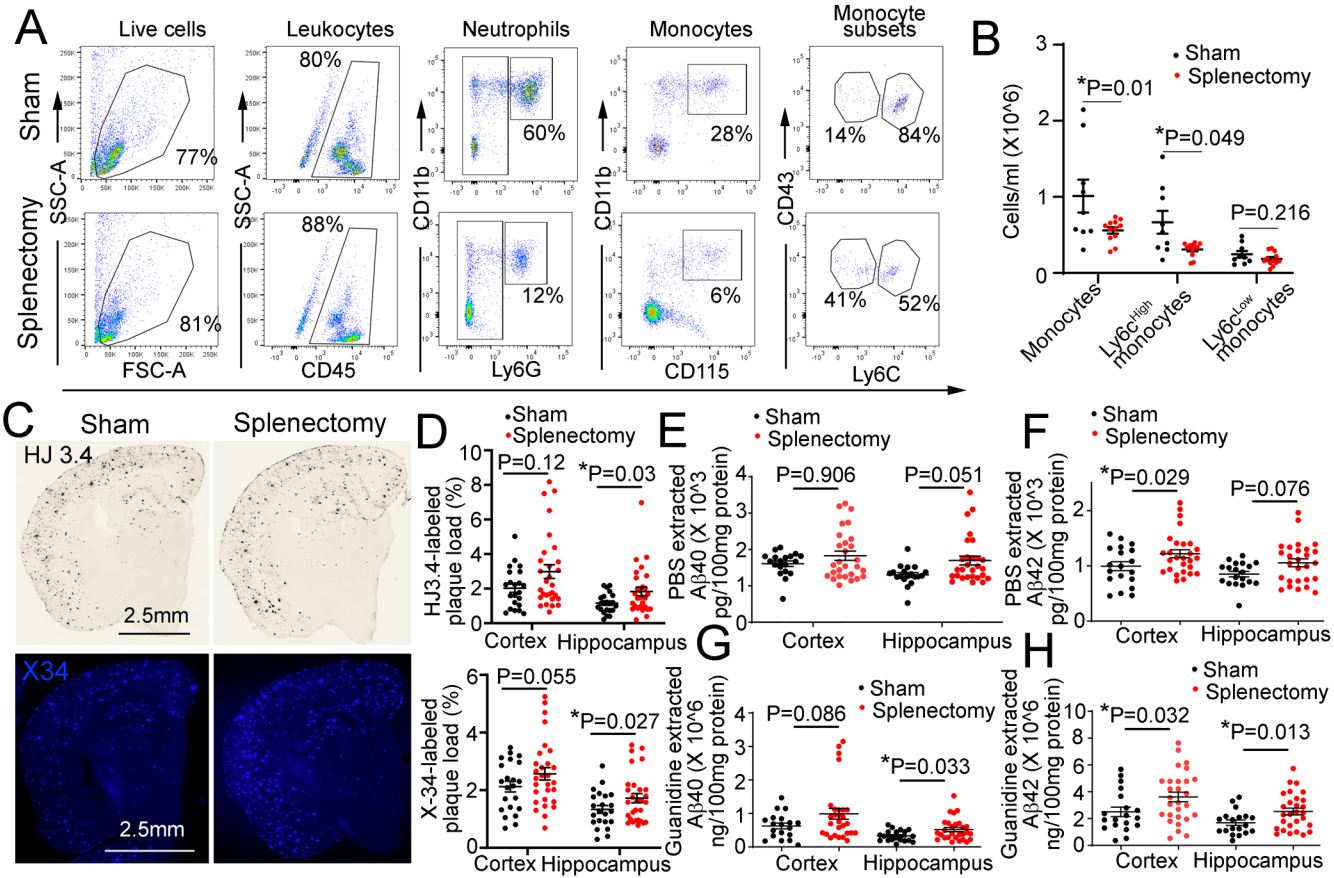
A
Live cells
Leukocytes
Neutrophils
Monocytes
Monocyte subsets
Sham
Splenectomy
SSC-A
FSC-A
CD45
CD11b
Ly6G
CD115
CD43
Ly6C
77%
80%
60%
28%
14%
84%
81%
88%
12%
6%
41%
52%
B
Sham
Splenectomy
Cells/ml (X10^6)
*P=0.01
*P=0.049
P=0.216
Monocytes
Ly6C^High monocytes
Ly6C^Low monocytes
C
Sham
Splenectomy
HJ 3.4
X34
2.5mm
D
HJ3.4-labeled plaque load (%)
P=0.12
*P=0.03
Cortex
Hippocampus
E
PBS extracted Aβ40 (X 10^3 pg/100mg protein)
P=0.906
P=0.051
F
PBS extracted Aβ42 (X 10^3 pg/100mg protein)
*P=0.029
P=0.076
X-34-labeled plaque load (%)
P=0.055
*P=0.027
G
Guanidine extracted Aβ40 (X 10^6 ng/100mg protein)
P=0.086
*P=0.033
H
Guanidine extracted Aβ42 (X 10^6 ng/100mg protein)
*P=0.032
*P=0.013

Figure 5: Splenectomy reduces circulating myeloid cells, and worsens amyloid pathology. A, B. Flow-cytometric phenotyping strategy (A, after doublet exclusion was performed) for assessment of total white blood cells, monocytes (total, and separately as Ly6cHigh and Ly6cLow) and polymorphonuclear neutrophils (PMNs) in APP/PS1 female mice 4 months post-splenectomy vs. matched sham-operated controls. Grouped data for total monocytes, and Ly6cHigh and Ly6cLow monocytes is shown in B. N=13 splenectomy; N=9 sham. P values are by t-test, except for comparison of Ly6cHigh monocytes by Wilcoxon rank sum test. **C, D.** Representative images (C) of HJ3.4 (anti-Aβ antibody) stained (top) and X-34 stained compact amyloid plaques (bottom); with quantitation (D) of plaque load in the cortex (Ctx) and hippocampus (Hpx) by HJ3.4 staining (top) and X-34 staining (bottom) in female APP/PS1 mice after splenectomy. N=22 post-splenectomy; N=29 post-sham procedure. P values are by t-test for panel D, except for comparison of X-34 stained plaques in hippocampus where a Wilcoxon rank sum test was employed. **E-H.** Quantitative assessment of Aβ40 and Aβ42 levels in PBS-extracted and guanidine extracted brain tissue (cortex: Ctx and hippocampus: Hpx) from APP/PS1 subjected to splenectomy as in D. N=26 post-splenectomy; N=21 post-sham procedure. P values are by Wilcoxon rank sum test for panel E; and by t-test for panels F-H, except for comparison of Aβ42 levels in hippocampus in panel F where Wilcoxon rank sum test was employed. * indicate $P<0.05$ for panels B, D-H.

Table 1: Contribution of GFP+ cells to cellular populations in the brain parenchyma.

Group (row)/ Cell type as a fraction of total population (column)	**Wild Type**	**APP/PS1**
GFP+/Iba1+	0%	2.16±0.44%
GFP+/CD11b+	0%	5.87±1.05%
GFP+/CD68+	0%	4.77±0.64%

All data are Mean±SEM.